Received: 13 June 2017 | Revised: 7 September 2017 | Accepted: 10 September 2017

DOI: 10.1002/adv.21908

RESEARCH ARTICLE

WILEY

PAA/alumina composites prepared with different molecular weight polymers and utilized as support for nickel-based catalyst

Peng Zhou[1] | Song Wang[1] | ChuanLan Tao[1] | Xingkui Guo[2] | Luhan Hao[3] | Qian Shao[2] | Lei Liu[1] | Ya-Ping Wang[1] | Wei Chu[1] | Bin Wang[1] | Shi-Zhong Luo[1] | Zhanhu Guo[3]

[1]School of Chemical Engineering, Sichuan University, Chengdu, Sichuan, China

[2]College of Chemical and Environmental Engineering, Shandong University of Science and Technology, Qingdao, Shandong, China

[3]Department of Chemical and Biomolecular Engineering, University of Tennessee, Knoxville, TN, USA

Correspondence
Bin Wang and Shi-Zhong Luo, School of Chemical Engineering, Sichuan University, Chengdu, Sichuan, China.
E-mails: bin_wang@scu.edu.cn; luosz@scu.edu.cn
and
Zhanhu Guo, Department of Chemical and Biomolecular Engineering, University of Tennessee, Knoxville, TN, USA.
E-mail: zguoz10@utk.edu

Abstract

Mesoporous alumina, as a porous, high specific surface area, high activity, and heat stable material, has been widely used as an industrial adsorbent, catalyst, and catalyst support. The modification of alumina with organic polymers has been widely investigated in recent years. In this study, we compared the dependence of the adsorption of a polyelectrolyte, poly(acrylic acid) (PAA) on γ-alumina particles on polymer size via Fourier transform infrared spectroscopy, thermogravimetry, nitrogen adsorption–desorption isotherm analysis, and atomic absorption spectrophotometry. We found that PAA with a hydrodynamic diameter greater than the alumina pore size would only adsorb on the outer surface of the oxides. For polymers with hydrodynamic diameters smaller than the alumina pore size, PAA infiltration resulted in a monolayer coverage of both the outer and inner surfaces of the oxide. Among the three PAA that could infiltrate the alumina pores, the one with the smallest molecular weight showed the highest adsorbed amount on alumina. The temperature, pH, concentration, and ionic strength of the PAA solutions were varied to illustrate the physicochemical differences of the prepared polymer/oxide composite materials. The high PAA-loaded composites were treated with a nickel ion solution, converted to Ni/alumina catalysts, and used in the methanation of carbon dioxide. The Ni/alumina catalysts were analyzed with X-ray diffraction and temperature-programmed reduction to illustrate the structural characteristics. The catalytic CO_2 methanation of the catalyst samples revealed that a solution pH value higher than pK_a of PAA favored the formation of catalysts with high catalytic activity.

KEYWORDS

catalysts, colloids, nanocomposites, nanoparticles, polyelectrolytes

1 | INTRODUCTION

Alumina is among the most studied metal oxide colloids that has been widely utilized in water purification to remove dissolved inorganic and organic contaminants. The alumina surface is complex and contains several types of surface hydroxyl groups for adsorption and surface reaction.[1] Dry alumina would have only oxygen atoms on the top layer usually over aluminum atoms in octahedral sites in the next lower layer. Alumina is a white powder with various crystal phases. The reported isoelectric point for alumina is between pH 7.2 and 9. Among the three common alumina crystal phases, γ-Al_2O_3

is termed the active alumina. It has a specific surface area of 100–300 m^2/g that is the reason for its very high adsorption capacity.[2] It is mechanically and thermally stable, a common feature of all alumina crystal phases. γ-Al_2O_3 has been employed in the applications such as adsorbent, dehydrant, specialty ceramics, catalyst and catalyst support in chemical industries and petroleum refining. γ-Al_2O_3 belongs to the cubic crystal system and is formed by heating boehmite AlO(OH) between 400 and 500°C.

Even though it has been widely used, much effort is devoted to further increase the surface properties of alumina. A template method has been attempted to create alumina with higher specific surface area and better pore size control.[3,4] In this approach, surfactants are used as the organic template and aluminum alkoxides as the starting materials to generate alumina colloids with very high specific surface areas. But the overall complex procedure and the high cost make this approach not commercially competitive. The adsorption feature of alumina colloids depends on the hydroxyl groups present on the surface.[5] These hydroxyl groups can form hydrogen bonds with certain functional groups of organic molecule to lead the formation of evenly dispersed organic layer on oxide support.[6,7] Polymers with functional groups have been effectively adsorbed onto alumina colloid surface.[8] Different from small organic molecules, polymers adsorbed on alumina colloid surface demonstrate distinct features that are related not only to the functional groups attached to the main chain, but also to the conformation adopted by the polymer molecules.[9,10] If the polymer contains charges, that is, a polyelectrolyte, electric repulsion along the chains greatly determines the chain conformation in solution. Ionic strength and solution pH are critical factors to influence the polyelectrolyte conformation, which in turn is closely related with the formation of the particle–polymer composite system.[11] For polymer chains with small molecular weight (M_W), the polymers can diffuse fast and adsorb onto the colloid surface first. If present, polymer chains with higher M_W will replace chains with the smallest M_W because of preferable entropies. After this stage, polymer chains with even higher M_W may not adsorb onto the colloid surface because the surface is covered with polymers with the same charge, thus repulsing further polymer adsorption.

Caruso et al.[12–14] have systematically studied the adsorption properties of polyelectrolyte into metal oxide mesoporous pores. Their studies conclude that the factor of polymer size versus pore size is the most influential for the polymer infiltration in nano/mesoporous particles. Large pores are capable to adsorb a broad range of molecular weight polymers. A coiled polymer conformation, adjusted by varying solution pH and ionic strength, in solution favors higher loadings on particles. The confined macromolecules adopt a more coiled conformation within the pores compared to that adsorbed on the particle surface. Poly(acrylic acid) (PAA) is a weak polyelectrolyte that has wide industrial applications.[15] Its high solubility in water bestows the safe utilization in many everyday products such as foods, cosmetics, detergents, and pharmaceuticals. For PAA chains with small molecular weight, the polymers may enter oxide pores within a certain pH range.[16] When the solution pH is too low, the coiled chains primarily reside on the outside surface. When the pH is too high, the oxide surface starts to bear negative charges impeding further adsorption of polymers. The small M_W polymers may cover the oxide inner surface evenly with a thickness of ~1.0 nm. In our own work,[17] we find a similar trend. At low pH, coiled PAA molecules primarily reside on the outer surface of γ-alumina. At high pH, stretched PAA chains can effectively infiltrate the oxide mesopores. In Caruso's work, the PAA infiltration behavior into oxide particle pores was investigated.[12] PAA molecules with average hydrodynamic diameter smaller than the oxide particle pore size can be regarded as fully infiltrating the inside of the particles, and the polymer adsorption isotherms reach a plateau at saturation. For the polymers with larger diameters than the pore size, the adsorbed amount increases almost linearly with increasing pore size.

One of the potential applications of the PAA/alumina composites is to act as the heterogeneous catalyst support to deposit the active phase. Metal ion sorption in the polymer/oxide composites is different than that with either component alone. When used together with oxides, PAA can either increase metal ion sorption by offering negative charge and/or complexation sites, or decrease sorption by blocking sorption sites on the surface. Brown Jr. et al.[18] studied Pb^{2+} and Zn^{2+} sorption and partitioning on PAA/γ-alumina. PAA significantly helped adsorption of metal ions, as metal ions reside predominantly within the PAA layers. Metal ion sorption onto PAA and alumina colloid surface is described by apparent stability constants. The sorption stability constant of metal ions with PAA was higher than the value of the sorption stability constant of metal ion with alumina.

Large-scale industrial operations such as hydrogenation, catalytic cracking, naphtha reforming, ethylene oxidation, and ammonia synthesis, to name a few, commonly use heterogeneous catalysts.[19] Market competition drives these industries to search for better performing catalysts, which has led to the development of an important class of heterogeneous catalysts involving nanoparticles of an active species supported on oxides having a high surface area.[20] Impregnation is a method applied throughout industry because it is a simple, economic, and usually reproducible way to form supported metal nanoparticle catalysts.[21] However, this method is not without pitfalls, some of which may lead to inconsistent performance.[22,23] Usually there is lack of a specific interfacial binding mechanism during the impregnation preparation, in which case the metal precursor

species can migrate on the support surface during the treatments after adsorption, causing inhomogeneous dispersions.[24] Also, support material surface irregularities, such as exposed crystal facets, phases, and defect structures, will influence precursor adsorption.[24] To circumvent the inhomogeneously produced active phase, loading of preformed metal nanoparticles onto support has been attempted. But this approach suffers from only being capable to deposit relatively small amounts of nanoparticles[25,26] as well as the irreproducible nature of the nanoparticle preparation.[23] In addition, remaining organic ligands binding to the nanoparticles during the preparation can result in relatively poor catalytic properties.[27] These issues generate inconsistencies in nanoparticle size, composition, distribution, and performance. An imperative need is to create supported catalysts with consistently uniform distribution of the active phase that provide improved performance. Current industrial efforts center on improvements for the in situ generation of the active nanoparticles. A few studies have explored the utilization of metal–polyelectrolyte complexes in assisting the synthesis of metal nanoparticles on oxide support. The layer-by-layer self-assembly method was employed to prepare a metal–polyelectrolyte complex layer wrapping around alumina particles.[28,29] Following reduction, this wrapping helped to obtain well-dispersed metal nanoparticles with a narrow size distribution.

We set out to produce catalyst samples based on the use of PAA as a coordination agent for the efficient formation of supported nanoparticles. We first prepare PAA/alumina composites to reveal the relationship between PAA M_W and polymer infiltration during the adsorption process. The PAA with a certain M_W is demonstrated to have the high adsorbed amount and therefore is used in the following experiments. Temperature, pH, concentration, and ionic strength of the PAA solutions are examined next to provide the optimum parameters for the preparation of PAA/alumina composites. We use CO_2 methanation[30] as the reporter reaction to test the proposed novel catalyst fabrication method. Systems based on nickel nanoparticles supported on alumina, usually prepared via the impregnation method, have been the preferred industrial catalysts for this reaction.[31] In this study, we prepare alumina-supported Ni catalysts as the proof-of-concept example to test the effects of polyelectrolyte infiltration on nanoparticle formation, and catalytic behavior of the nanoparticles in CO_2 methanation.

2 | MATERIALS AND METHODS

2.1 | Materials

γ-Al_2O_3 with 40–60 mesh (Tianjin Kemiou Chemicals Co.) was heated at 500°C in air for 3 hr for activation. Poly(acrylic acid) with M_W 800–1000 (denoted P_{1k} in the study) was purchased from Tianjin Kemiou Chemicals Co. in 30% (weight) solution. Poly(acrylic acid) with M_W 3,000 (P_{3k}) was acquired from Shanghai Aladdin Reagents Co. in 50% solution. Sodium polyacrylate with M_W 15,000 (P_{15k}) and poly(acrylic acid) with M_W 100,000 (P_{100k}) were supplied by Sigma–Aldrich (Shanghai) in 35% solutions. $Ni(NO_3)_2$, $NaNO_3$, NaOH, and HCl were analytical reagents. Water with conductivity $\leq$10 μs/cm was used throughout the experiments.

2.2 | Preparation of PAA/alumina composites with different PAA molecular weights

PAA solutions of 0.003, 0.1, and 0.3 M (0.216, 7.2, 21.6 g/L) were adjusted to pH 6.0–6.1 with either NaOH or HCl. At this pH range, PAA molecules were in ionic form.[17] To 10 ml of a PAA solution, 0.3 g of activated alumina was added and shaken for 12 hr. The solid was filtered and rinsed with water three times, then dried in air at 60°C overnight. The composite samples prepared with polymers samples P_{1k}, P_{3k}, P_{15k}, and P_{100k} were labeled C_{1k}, C_{3k}, C_{15k}, and C_{100k}, respectively.

2.3 | Preparation of PAA/alumina composites with different operational parameters

PAA with a certain M_W (1k) was used in the following experiments because C_{1k} was found to have the highest adsorbed PAA amount among composites prepared. Four PAA solution parameters were tested in the preparation of composites, solution pH (3 and 6), temperature (R.T. and 100°C), PAA concentration (0.01 and 0.1 M), and ionic strength (with and without 0.1 M $NaNO_3$). The preparation parameters are described in detail in Results and Discussion section. The composite samples were labeled P/Ax (x = 1–12), while the numerical order was chosen arbitrarily.

2.4 | Preparation of supported Ni catalysts from PAA/alumina composites

The incipient wetness method was employed to adsorb Ni^{2+} onto PAA/alumina composite samples P/Ax (x = 1–12) with a 5% Ni (weight) loading. After drying the samples at 110°C overnight, the materials were calcined at 450°C in air for 5 hr to produce supported nickel nanoparticle catalysts. The formed catalysts Ni/Ax (x = 1–12) were named according to the binary PAA/alumina samples P/Ax (x = 1–12). A control sample Ni/A was prepared in which Ni was directly loaded onto untreated alumina with the same manipulations as those of Ni/Ax.

2.5 | Catalytic CO_2 methanation performance of supported Ni catalysts

A continuous flow fixed-bed reactor operated at 0.1 MPa was used to test catalytic performance of the Ni/A*x* catalysts. Feed and product gas analysis was performed in a gas chromatograph (GC-1690, Hangzhou Kexiao Instrument) equipped with a thermal conductivity detector. The equipment was calibrated by adding 1 μl of H_2, CH_4, or CO_2 under reaction pressure and analyzing the individual peak position and area. For each catalytic activity run, about 200 mg of catalyst was loaded into a quartz reactor and reduced in situ under a continuous flow of H_2 at the rate of 40 ml/min at 600°C for 1 hr at a heating rate of 10°C/min, normal pressure of one bar, and GHSV of 15,000 ml h^{-1} $g_{cat}{}^{-1}$. The catalyst was cooled to 100°C, and a CO_2 flow of 10 ml/min was added to the H_2 flow. The catalytic CO_2 conversion reaction was carried out in the temperature range 240–420°C with a reactant flow rate of 50 ml/min of H_2/CO_2 (4:1) mixture. The reaction was equilibrated at each temperature point for at least 30 min to provide gas sample for GC analysis. The temperature points used were 240, 270, 300, 320, 340, 360, 380, 400, and 420°C. Temperature-programmed reduction (TPR) analysis was conducted on the same setup for catalytic performance to determine the reducibility of the catalysts. About 50 mg of catalyst was placed in the quartz reactor, and the temperature was raised from 100 to 800°C at a heating rate of 10°C/min under a 5% H_2/N_2 flow stream of 30 ml/min. The amount of hydrogen consumed was determined online using a gas chromatograph (SC-200, Chongqing Chuanyi Jiuchang) equipped with a thermal conductivity detector.

2.6 | Characterization

Room temperature Fourier transform infrared (FT-IR) spectroscopy (Perkin Elmer Spectrum Two) was acquired from KBr pellets, of which ~1 wt.% was the sample, in the range of 4,000–400 cm^{-1}. X-ray diffraction (XRD) patterns were acquired on a Philips X'pert PRO diffractometer using Cu Kα radiation (45 kV, 50 mA).[32] Samples were scanned between 10 and 80° (2θ) at a scan step size of 0.03° and scan time constant of 2 s per step. The Ni crystallite size (dXRD) was determined by X-ray line broadening analysis according to the Scherrer method. Thermogravimetry (TG) (HCT-2 Differential Thermal Balance, Beijing Hengjiu Scientific Instrument Co.) was operated in the range of 80–700°C in air with a heating rate of 10°C/min.[33,34] The specific surface areas, total pore volumes, and average pore diameters were determined from the nitrogen adsorption–desorption isotherms at −196°C, which were measured using an automated surface area and pore size analyzer (Quantachrome NOVA 1000e). Before each measurement, the samples were degassed in vacuum at 200°C for 3 hr. Specific surface areas of samples were calculated by the Brunauer–Emmett–Teller (BET) method, and the pore size distribution and average pore diameter were determined according to the Barrett–Joyner–Halenda (BJH) method applied to desorption isotherms.

3 | RESULTS AND DISCUSSION

3.1 | PAA Adsorption Behavior Corresponding to Polymer Size

According to a literature report,[35] the commercial PAA samples chosen for this study presumably have the following average hydrodynamic diameters based on their respective molecular weight (M_W): P_{1k}, 1.9 nm; P_{3k}, 3.2 nm; P_{15k}, 6.8 nm; and P_{100k}, 18 nm. The measured average pore diameter of alumina particles is 9.6 nm (Table 1). Thus, we would expect that samples P_{1k} and P_{3k} should be able to completely infiltrate the oxide pores and sample P_{100k} would not. Sample P_{15k} has a hydrodynamic diameter close to the average pore size of the oxide and may exhibit unique adsorption behavior. In the preparation of PAA/alumina hybrids, we chose three PAA concentrations of 0.003 M (0.216 g/L), 0.1 M (7.2 g/L), and 0.3 M (21.6 g/L). PAA/alumina hybrids with high PAA loadings are assumed to have relatively high metal ion sorptivity, while very low PAA concentrations are not expected to provide such hybrid samples. The lowest concentration, 0.003 M, was chosen as a representative of low PAA concentrations, while the highest concentration, 0.3 M, was selected considering that some commercial PAA solutions are supplied at 0.6 M (30%). The polymer adsorption was carried out at pH 6 to ensure high electrostatic attraction between PAA and alumina.

Table 1 presents the physicochemical characteristics of pristine alumina and hybrid C_{15k} samples. The pristine γ-Al_2O_3 had a specific surface area S_{BET} of 169.3 m^2/g, measured via N_2 sorption and desorption. Upon adsorption of P_{15k} from solution at pH 6, the sample demonstrated an S_{BET} of 164.9 m^2/g, illustrating the coverage of oxide surface area by

TABLE 1 Physicochemical characteristics of pristine alumina and composite samples prepared using P_{15k} with or without added 0.1 M $NaNO_3$, and calculated values which assumed uniform coverage of PAA on alumina surface

Sample	S_{BET} (m^2/g)	Pore volume (ml/g)	Pore diameter (nm)
γ-Al_2O_3	169.3	0.405	9.6
C_{15k}, no-salt	164.9	0.385	9.3
cal.	164.0	0.380	9.3
C_{15k}, salt	155.9	0.344	8.8
cal.	159.0	0.357	9.0

adsorbed polymer. The sample was also tested using thermogravimetry (TG) (plot not shown). Assuming the mass loss in the range of 200–500°C belonged to organic matter, that is, PAA, and the polymer coverage of the oxide surface was evenly distributed, the calculated S_{BET} was 164.0 m^2/g using the method described in our recent publication, in which molecular PAA was in situ prepared via free radical polymerization of pre-adsorbed acrylic acid.[36] The measured value confirms the calculated value, suggesting the uniform coverage of PAA on alumina surface.

The FT-IR spectra of PAA/alumina hybrid samples prepared with different M_W PAA are shown in Figure 1. Panel A shows the curves of, from lower to upper, pristine alumina, hybrid sample C_{1k} prepared with 0.003 M P_{1k} solution, C_{1k} prepared with 0.1 M P_{1k} solution, and C_{1k} prepared with 0.3 M P_{1k} solution, respectively. Panels B, C, and D demonstrate the similar curves for composites of P_{3k}, P_{15k}, and P_{100k}, respectively. The selected peak positions are illustrated in panel A, and they represent those in panels B, C, and D. Pristine alumina showed characteristic O—H bending vibration of adsorbed water at ~1,637 cm^{-1}, and the Al—OH bending at 1,385 cm^{-1}.[37] Incorporation with PAA presented characteristic —COO^- asymmetric stretching vibration at ~1,562 cm^{-1}, and the coupled symmetric —COO^- and deformed CH_2 at 1,410 cm^{-1}.[38] The difference between ν_{as} and ν_s of the —COO^- group suggests a bridging mode.[39] Adsorbed PAA also showed substantial absorbance at 1,385 cm^{-1}, similar to our previous report.[36]

The dependence of both PAA adsorption amount PAA_{ads} and surface area coverage Γ_{PAA}, measured via TG, of the four PAA/alumina composite samples on the concentration of PAA is presented in Table 2. For C_{1k}, C_{3k}, and C_{15k}, the

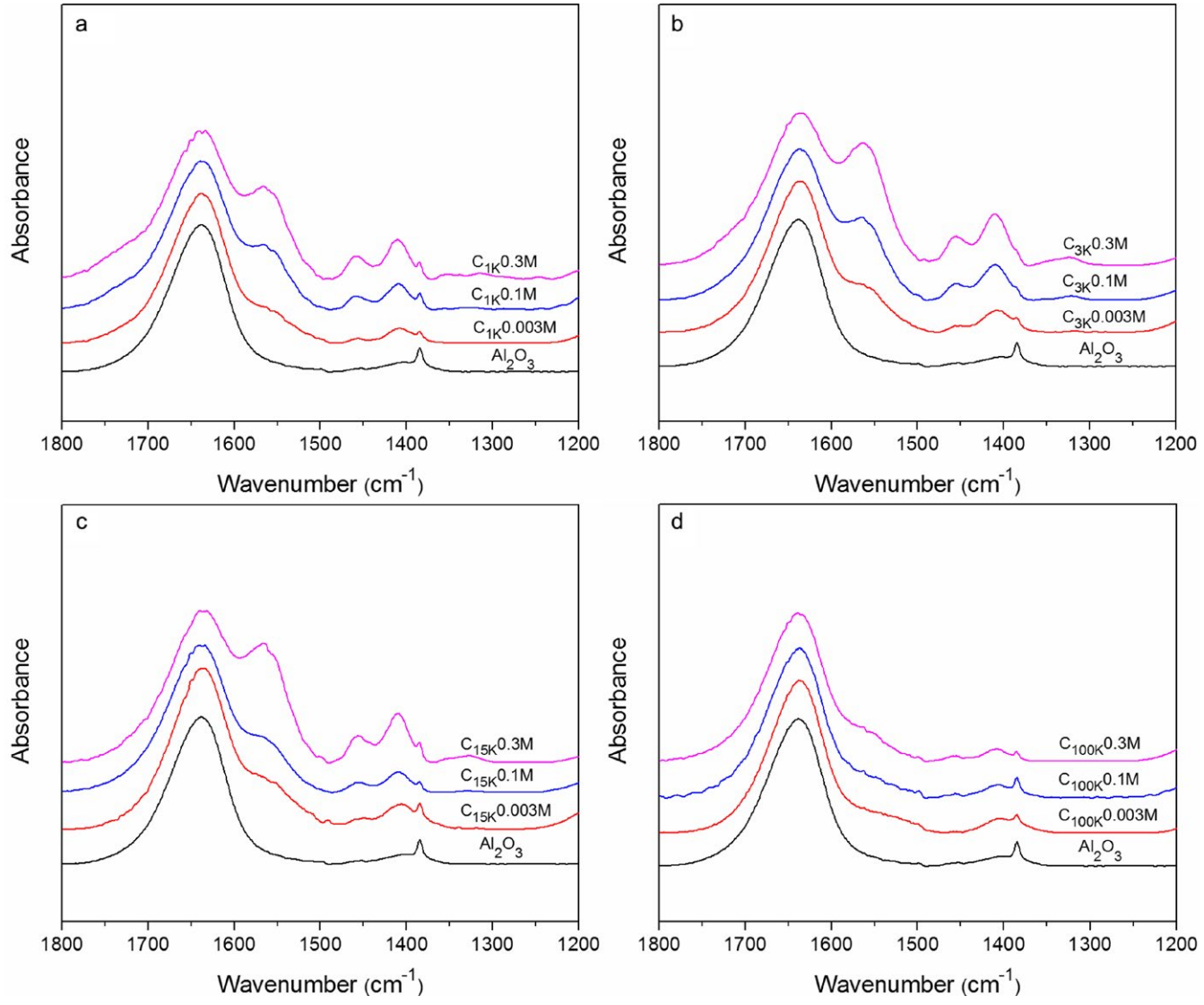

FIGURE 1 Panel a: FT-IR spectra of the curves of, from lower to upper, pristine alumina, composite sample C1k prepared with 0.003 M P1k solution, C1k prepared with 0.1 M P1k solution, and C1k prepared with 0.3 M P1k solution, respectively. Panels b, c, and d demonstrate the similar curves for composites prepared with P3k, P15k, and P100k, respectively [Colour figure can be viewed at wileyonlinelibrary.com]

TABLE 2 PAA adsorption amount PAA_{ads} and surface PAA coverage Γ_{PAA} on alumina in hybrid samples prepared with different PAA concentrations, and corresponding layers of PAA on alumina surface of composite samples

Sample	PAA_{ads} (mg/g)	Γ_{PAA} (μg/m^2)	Monolayer[c]
C_{1k}[a]			
0.003 M	16.35	96.58	0.3
0.1 M	41.51	245.2	0.8
0.3 M	70.70	417.6	1.4
C_{3k}[a]			
0.003 M	15.55	91.84	0.3
0.1 M	40.07	236.7	0.8
0.3 M	60.12	355.1	1.2
C_{15k}[a]			
0.003 M	11.38	67.23	0.2
0.1 M	30.46	179.9	0.6
0.3 M	48.10	284.1	0.9
C_{100k}[b]			
0.003 M	16.67	964.8	3.1
0.1 M	17.15	992.6	3.2
0.3 M	17.47	1011	3.3

[a]Assuming PAA adsorption both inside and outside oxide pores.
[b]Assuming PAA adsorption only outside oxide pores.
[c]Calculated based on data from Ref.[37]

adsorbed PAA was presumably evenly distributed on both the outer and inner surfaces of alumina particles. The adsorbed PAA for the three samples increased with higher PAA concentrations, and the overall PAA_{ads} values for these samples were higher than that of C_{100k}, in which PAA should only cover the outer surface of alumina particles. The surface area coverage Γ_{PAA} was calculated using the measured S_{BET} value of pristine alumina for C_{1k}, C_{3k}, and C_{15k}. For C_{100k}, the large polymer hydrodynamic diameter should effectively prevent it from infiltrating the oxide pores, so the adsorption would take place at the outer surface of alumina particles. According to the supplier, the γ-Al_2O_3 sample had a particle diameter of 0.5 μm and a density of 0.70 g/cm^3, translating into a calculated alumina outer surface area of 17.28 m^2/g. The commercial alumina sample (40–60 mesh, 425–250 μm) should be agglomerates of individual particles. We assume the operation had broken up the agglomerates so the surface coverage could be calculated for comparison. The calculated surface coverage Γ_{PAA} values of the four hybrids also show that P_{100k} covered the oxide surface in a different fashion to the other three PAA samples. The C_{100k} had much higher Γ_{PAA} values across the PAA concentration range than other hybrid samples, and the Γ_{PAA} value fluctuation was negligible. If assuming a monolayer PAA coverage of 337.8 μg/m^2 according to Ref.,[40] the C_{100k} would have a three-monolayer PAA coverage on the oxide outer surface. Two possibilities could explain the origin of this three-monolayer PAA coverage. One is that the polymer adopts the stretched conformation and lays on the oxide outer surface in a stratified fashion. In this case, the electrostatic attraction between carboxylate groups of PAA and the positively charged alumina surface (isoelectric point of pH 7.2–9) is the major contributor for the adsorption. The second possibility is that PAA molecules existed in a coiled conformation so the adsorbed layer was thicker than a stretched monolayer. However, the polymer adsorption process was taking place with no added ionic strength. Therefore, the polyelectrolyte chains would keep the relatively stretched conformation in solution. Because of the lack of evidence demonstrating that polyelectrolyte adsorption onto oppositely charge oxide surface would change the polymer conformation from stretched to coiled, the first scenario that the electrostatic force extended to three monolayers of PAA is preferable. The PAA adsorption value in our study is one order of magnitude higher than that reported in the literature with a value of about 3.8 mg/g for the M_W 60,000 g/mol sample[41] in which a PAA concentration of 100 ppm was used. In that study, the low PAA adsorption is attributed to the low polymer concentration.

For the other three samples, the PAA_{ads} showed a similar pattern, increasing with higher PAA concentrations. For higher M_W, PAA_{ads} tended to be smaller because the bigger molecules would encounter increased infiltration resistance. Γ_{PAA} also grew upon increasing PAA concentrations. At the highest PAA concentration of 0.3 M, C_{1k}, C_{3k}, and C_{15k} reached a PAA coverage of around one monolayer, both inside and outside the oxide pores, Table 2. The one-monolayer coverage of the inner surface is consistent with the electrostatic interaction between PAA and alumina surface via the bridging mode. After this stage, the diffusion resistance within the confined cavity became too great to overcome at this stage. Therefore, only a one-monolayer coverage was observed within the alumina mesopores.

The equilibrium adsorption isotherms of the four PAA samples on alumina are shown in Figure 2 as the dependence of adsorbed PAA amount PAA_{ads} on the concentration of PAA. PAA adsorption on alumina has been well documented to follow the Langmuir model,[42] in which the slope at the onset of adsorption isotherms represents the affinity of a polymer for the surface. For P_{100k}, the adsorption process appeared to reach the plateau at saturation even at the lowest tested PAA concentration of 0.003 M, indicating a very high affinity for the alumina outer surface. In the work of Mishael et al.,[43] when the polymer diameter is greater than the oxide pore size, the adsorption reached a plateau around 1.5 g/L polymer concentration. In our study, an adsorption plateau might have been reached at or below 0.003 M (0.216 g/L) for P_{100k} chains. For this polymer species, meaningful infiltration was severely hindered, and the adsorption was expected to take place on the outside surface of the oxide particles for

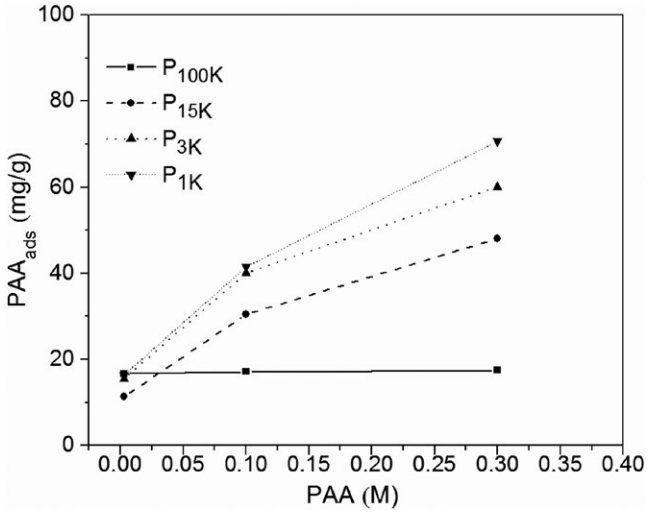

FIGURE 2 The dependence of PAA adsorption amount PAAads, measured via TG, on the concentration of PAA during the preparation of composite samples

polymers having a hydrodynamic diameter greater than the pore size. For the other three M_W polymers, the adsorption did not reach the saturation level within the experimental PAA concentration range. These polymers demonstrate a much lower affinity toward the inner surface of alumina particles, for example, much slower slope at the onset of the adsorption isotherms. The lower affinity can be attributed to the much higher resistance for the polymers to enter the oxide pores.

3.2 | Ni/A*x* catalysts preparation and performance in CO_2 methanation reaction

The preparation of P/A*x* composite samples was conducted preceding to the preparation of Ni/A*x* catalyst samples. The above experiments demonstrate that among the four PAA samples with different M_W, using P_{1k} could afford composite sample C_{1k} with higher PAA adsorption amount than the other composites samples. Therefore, P_{1k} was used in the remaining preparation of composite samples P/A*x* (x = 1–12). PAA solution pH, temperature, concentration, and ionic strength were systematically varied in the preparation of P/A*x*, Table 3. Among the four parameters, PAA solution concentration had been varied in the preparation of composite samples C_y (y = 1k, 3k, 15k, 100k). PAA solution pH, temperature, and ionic strength were not tested in the above experiments. After preparation of the composite samples P/A*x*, the samples were used for the preparation of supported Ni catalyst samples Ni/A*x* (x = 1–12). Characterization and catalytic performance were carried out on the catalyst samples.

The powder X-ray diffraction (XRD) measurements of five representative samples were performed, and all peaks were identified with JCPDS files as shown in Figure 3. The five samples were chosen to compare the physicochemical

TABLE 3 Parameter variation in preparation of P/A*x*: PAA solution pH, temperature, concentration, and ionic strength

Sample	pH	Temp. (°C)	PAA conc. (M)	I.S. (M)
P/A1	6	R.T.	0.01	
P/A2	3	R.T.	0.01	
P/A3	6	R.T.	0.1	
P/A4	3	R.T.	0.1	
P/A5	6	100	0.1	
P/A6	6	100	0.01	
P/A7	3	100	0.01	
P/A8	3	100	0.1	
P/A9	6	R.T.	0.1	0.1
P/A10	6	100	0.01	0.2
P/A11	6	R.T.	0.01	0.2
P/A12	6	100	0.1	0.1

properties of samples whose preparation parameters were paired. The comparison of the five samples is based on the following differences: between samples Ni/A1 and Ni/A2, the influence of solution pH was tested; between Ni/A1 and Ni/A3, solution concentration; between Ni/A1 and Ni/A6, temperature; between Ni/A3 and Ni/A9, solution ion strength. The Ni {111}, {200}, and {220} crystal phases are found in all five samples along with alumina peaks, indicating the incorporation of Ni into Al_2O_3. The particle size of each sample was calculated according to the Scherrer method (Table 4). XRD results show that Ni nanoparticles in sample Ni/A9 were smaller in size than the other samples.

To evaluate the PAA influence on the catalyst performance, the temperature-programmed H_2 reduction (TPR) for the different nickel nanoparticle formation patterns of the

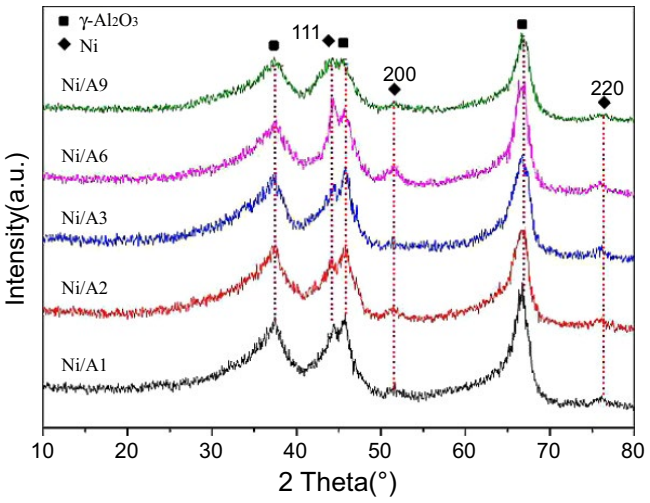

FIGURE 3 The powder X-ray diffraction (XRD) measurements of five representative samples with all peaks identified with JCPDS files [Colour figure can be viewed at wileyonlinelibrary.com]

TABLE 4 Particle size of five samples, prepared under varied PAA solutions, using data acquired in XRD and calculated according to the Scherrer method

Sample	pH	Temp. (°C)	Conc. (M)	I.S. (M)	Particle size (nm)			
					d111	d200	d220	d_a
Ni/A1	6	R.T.	0.01		6.5	13.7	12.4	10.87
Ni/A2	3	R.T.	0.01		6.6	13.6	13.7	11.3
Ni/A3	6	R.T.	0.1		6.8	13.8	9.9	10.17
Ni/A6	6	100	0.01		6.9	12.9	10	9.93
Ni/A9	6	R.T.	0.1	0.1	5.8	7.3	9.5	7.53

TABLE 5 Area percentages of NiO reduction peaks obtained from the TPR experiments in catalyst samples prepared under varied PAA solutions

sample	pH	Temp. (°C)	Conc. (M)	I.S. (M)	Peak area (%)		
					α	ß	γ
Ni/A1	6	R.T.	0.01		5.7	51.3	43
Ni/A2	3	R.T.	0.01		10.2	45.5	44.3
Ni/A3	6	R.T.	0.1		12.7	52.2	35.1
Ni/A6	6	100	0.01		5.3	59	35.7
Ni/A12	6	100	0.01	0.2	7.6	48.4	44

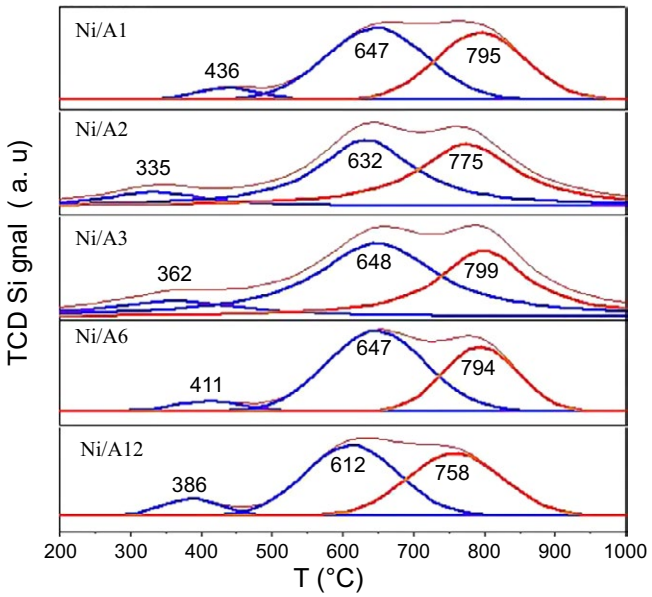

FIGURE 4 Temperature-programmed H_2 reduction (TPR) for the different nickel nanoparticle formation patterns of five samples, before in situ H_2 reduction, and the simulated area percentages of each sample [Colour figure can be viewed at wileyonlinelibrary.com]

five samples studied with XRD, before in situ H_2 reduction, is plotted with the simulated area percentages of each sample (Figure 4). This set of five catalyst samples is the same to that in the XRD study, except that Ni/A9 was replaced by Ni/A12. Nonetheless, both the pairing between Ni/A6 and Ni/A12 and that between Ni/A6 and Ni/A12 reveal the solution ionic strength effect. Each sample shows three reduction peaks that represent three nickel species:[44,45] α-, β-, and γ-NiO. Type α-NiO is easily reduced to form aggregated nanoparticles that contribute insignificantly to the catalytic activity. The nickel nanoparticles formed by reducing β-NiO are the fine ones that constitute the majority of active catalytic sites, while type γ-NiO is the less reducible in the Al-rich phase that is prone to form the inactive spinel $NiAl_2O_4$. The TPR results show that the percentage of β-NiO follows the order Ni/A6 > Ni/A3 ≥ Ni/A1 > Ni/A12 > Ni/A2 (Table 5). This order suggests that sample Ni/A6 would have the highest catalytic activity, while Ni/A2 would be the least active catalyst. Another feature is that the reduction of β-NiO took place apparently earlier in Ni/A12 than other samples, implying the easier formation of highly active Ni crystallites. For the other samples, the reduction peak for β-NiO occurred close to 650°C, while the experimental reduction temperature was set at 600°C. Therefore, these four samples might have more β-NiO, but the prolonged reduction could yield less than the corresponding percentage of active Ni crystallites.

Examination of the catalytic CO_2 methanation was conducted over a temperature range of 240–420°C. Figures 5 and 6 display the CH_4 yield versus temperature for 12 catalyst samples with 5% Ni loading. The two figures were divided according to the pH value of the PAA solution when P/A*x* was prepared: Figure 5 includes those prepared at pH 3, and Figure 6 contains those at pH 6. Across the temperature range, the sample catalysts performed similarly, producing more CH_4 at higher temperatures. It is very obvious that catalysts Ni/A*x* prepared from P/A*x* obtained at pH 6 had higher catalytic activity than control Ni/A, while those at pH 3 were less active than control. The result regarding PAA solution pH is in accordance with our recent work.[46] When

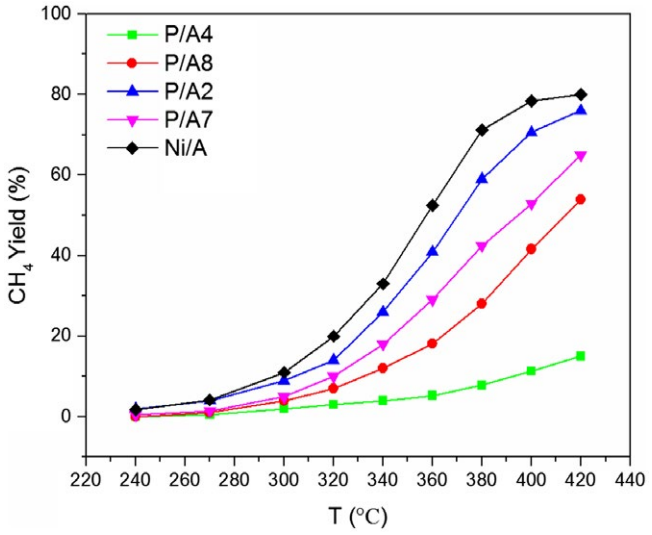

FIGURE 5 Effect of reaction temperature (240–420°C) on the catalytic performance of 5% Ni-loading catalyst samples using composites P/A*x* produced at pH 3 [Colour figure can be viewed at wileyonlinelibrary.com]

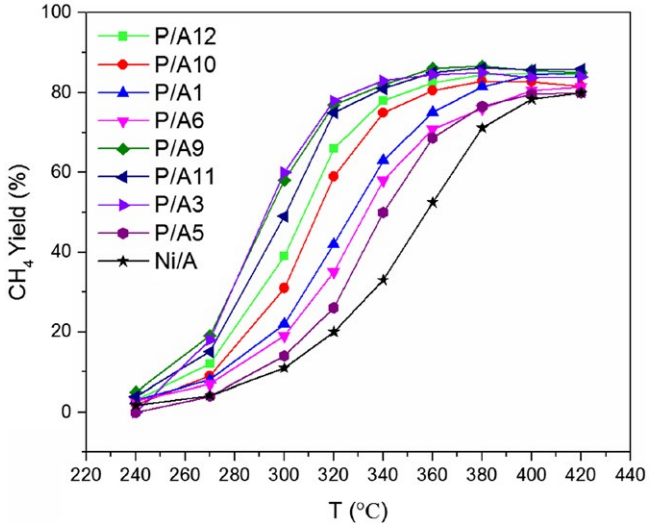

FIGURE 6 Effect of reaction temperature (240–420°C) on the catalytic performance of 5% Ni-loading catalyst samples using composites P/A*x* produced at pH 6 [Colour figure can be viewed at wileyonlinelibrary.com]

PAA was used at a pH < p*K*a, random coils of polymer were more compact because the side chains participated in more intramolecular hydrogen bonding. When alumina was pre-adsorbed with this PAA, the chains failed to cover the inner surface of pores. During the ion loading, the noncoordinating PAA chains competed for adsorption sites on alumina surface with Ni^{2+}, resulting in nickel deposition inferior to that of the system without using PAA. Following calcination, the nickel nanoparticle size, size distribution, and dispersion were large.

There are four pairs in the pairing catalyst samples to test the ionic strength effect. The front is the sample prepared without added $NaNO_3$, while the back is the sample prepared with $NaNO_3$: Ni/A1 vs. Ni/A11, Ni/A3 vs. Ni/A9, Ni/A5 vs. Ni/A10, and Ni/A6 vs. Ni/A12. Samples Ni/A3 and Ni/A9 had almost identical activities, and both were the most active among all catalyst samples. The other three pairs show a similar trend; that is, the sample prepared with added ionic strength showed higher catalytic activities. Therefore, under the P/A*x* composite preparation conditions, the addition of ionic strength helped the resulting catalysts to display high catalytic activity. We note that Ni/A9 had the smallest particle size via XRD analysis (Table 4). Thus, it suggests that better dispersion of the active phase helped produce high catalytic activity.

Next, we compare the pairs with a temperature difference, that is., a pair is placed together with the R.T. sample in front and the 100°C sample behind. The pairs are: Ni/A1 vs. Ni/A6, Ni/A2 vs. Ni/A7, Ni/A3 vs. Ni/A5, Ni/A4 vs. Ni/A8, Ni/A9 vs. Ni/A10, and Ni/A11 vs Ni/A12. Among the six pairs, only in the pair of Ni/A4 vs. Ni/A8, the sample prepared at 100°C, demonstrated a higher catalytic activity than the one prepared at R.T. Note that Ni/A4 showed an exceedingly low activity among all samples. Therefore, it is possible P/A*x* samples prepared at R.T. are more advantageous as support materials for the preparation of Ni/A*x*, although the effect is not shown at a substantial degree.

Finally, an analysis is carried out to determine the influences of PAA concentration on catalytic activity of Ni/A*x* samples. The front one is the sample with 0.01 M PAA solution, while the back one is the 0.1 M sample: Ni/A1 vs. Ni/A3, Ni/A2 vs. Ni/A4, Ni/A6 vs. Ni/A5, Ni/A7 vs. Ni/A8, Ni/A11 vs. Ni/A9, and Ni/A12 vs. Ni/A10. Among the six pairs, pairs Ni/A1 vs. Ni/A3 and Ni/A11 vs. Ni/A9 have the 0.1 M samples with higher activity, while the other four show the opposite trend, although sometimes the differences are very small. Both 0.01 and 0.1 M PAA concentrations behaved similarly as the support for Ni catalysts.

4 | CONCLUSIONS

Adsorption of PAA molecules with different molecular weights on mesoporous alumina was investigated. The PAA adsorption strongly depended on the polymer size. For polymers with a hydrodynamic diameter greater than the average alumina pore size, polymer adsorption was located solely on the outer surface of the oxide particles. For PAA with a hydrodynamic diameter smaller than the alumina pore size, the polymer chains would infiltrate the pores to be adsorbed on the inner surface of the oxide particles. PAA with the smallest molecular weight was used to prepare PAA/alumina composites that were subsequently used as the catalyst carriers to form supported Ni catalysts. PAA solution pH, temperature, concentration, and ionic strength were varied in the preparation. The produced catalysts were employed in the catalytic

CO_2 methanation reaction. When preparing the PAA/alumina composite, a polymer solution pH < pK_a seemed detrimental to the consequentially produced catalysts in terms of catalytic activity. To better coordinate with metal ions, the polymers would be in ionic instead of molecular form. On the other hand, the addition of ionic strength could lead to better catalytic performance. Within the experimental error scope, temperature and PAA concentration had relatively small effects on the performance of the ensuing catalysts. Meanwhile, this study provides an approach to fabricate multifunctional polymer nanocomposites with different polymer matrix or functional fillers.[47–62]

ACKNOWLEDGMENTS

The authors gratefully acknowledge financial support from SINOPEC Maoming Company.

ORCID

Ya-Ping Wang http://orcid.org/0000-0002-3308-4728
Bin Wang http://orcid.org/0000-0002-1447-7577

REFERENCES

[1] S. Bertazzo, K. Rezwan, *Langmuir* **2010**, *26*, 3364.
[2] G. W. Kabalka, R. Pagni, *Tetrahedron* **1997**, *53*, 7999.
[3] S. Cabrera, J. El Haskouri, J. Alamo, A. Beltrán, D. Beltrán, S. Mendioroz, M. D. Marcos, P. Amorós, *Adv. Mater.* **1999**, *11*, 379.
[4] Z. Shan, J. C. Jansen, W. Zhou, T. H. Maschmeyer, *Appl. Catal. A* **2003**, *254*, 339.
[5] P. J. Eng, T. P. Trainor, G. E. Brown Jr, G. A. Waychunas, M. Newville, S. R. Sutton, M. L. Rivers, *Science* **2000**, *288*, 1029.
[6] M. E. Karaman, D. A. Antelmi, R. M. Pashley, *Colloids Surf. A* **2001**, *182*, 285.
[7] C. E. Taylor, D. K. Schwartz, *Langmuir* **2003**, *19*, 2665.
[8] A. A. Zaman, R. Tsuchiya, B. M. Moudgil, *J. Colloid Interface Sci.* **2002**, *256*, 73.
[9] J. Sun, L. Bergström, L. Gao, *J. Am. Ceram. Soc.* **2001**, *84*, 2710.
[10] Z. Pan, A. Campbell, P. Somasundaran, *Colloids Surf. A* **2001**, *191*, 71.
[11] M. Wiśniewska, S. Chibowski, T. Urban, *Appl. Surface Sci.* **2014**, *320*, 843.
[12] Y. Wang, A. S. Angelatos, D. E. Dunstan, F. Caruso, *Macromolecules* **2007**, *40*, 7594.
[13] A. S. Angelatos, Y. Wang, F. Caruso, *Langmuir* **2008**, *24*, 4224.
[14] G. L. Drisko, L. Cao, M. C. Kimling, S. Harrisson, V. Luca, F. Caruso, *ACS Appl. Mater. Interfaces* **2009**, *1*, 2893.
[15] D. Reith, B. Müller, F. Müller-Plathe, S. Wiegand, *J. Chem. Phys.* **2002**, *116*, 9100.
[16] S. Chibowski, M. Wiśniewska, A. W. Marczewski, S. Pikus, *J. Colloid Interface Sci.* **2003**, *267*, 1.
[17] L. Liu, S.-Z. Luo, B. Wang, Z. Guo, *Appl. Surface Sci.* **2015**, *345*, 116.
[18] Y. Wang, F. M. Michel, C. Levard, Y. Choi, P. J. Eng, G. F. Brown Jr, *Environ. Sci. Technol.* **2013**, *47*, 12131.
[19] J. E. Mondloch, E. Bayram, R. G. J. Finke, *Molecul. Catal. A* **2012**, *355*, 1.
[20] P. C. Stair, *J. Chem. Phys.* **2008**, *128*, 182507/1.
[21] M. Campanati, G. Fornasari, A. Vaccari, *Catal. Today* **2003**, *77*, 299.
[22] Y. Huang, Y. Li, P. Cheng, H. Chen, R. Li, X. Li, C. W. Yip, A. S. C. J. Chan, *Molecul. Catal. A* **2002**, *189*, 219.
[23] R. H. Crabtree, *Chem. Rev.* **2012**, *112*, 1536.
[24] A. Y. Khodakov, W. Chu, P. Fongarland, *Chem. Rev.* **2007**, *107*, 1692.
[25] C.-K. Tsung, J. N. Kuhn, W. Huang, C. Aliaga, L.-I. Hung, G. A. Somorjai, P. Yang, *J. Am. Chem. Soc.* **2009**, *131*, 5816.
[26] M. Cargnello, V. V. T. Doan-Nguyen, T. R. Gordon, R. E. Diaz, E. A. Stach, R. J. Gorte, P. Fornasiero, C. B. Murray, *Science* **2013**, *341*, 771.
[27] R. Rinaldi, A. D. M. Porcari, T. C. R. Rocha, W. H. Cassinelli, R. U. Ribeiro, J. M. C. Bueno, D. J. Zanchet, *Molecul. Catal. A* **2009**, *301*, 11.
[28] S. Kidambi, J. Dai, J. Li, M. L. Bruening, *J. Am. Chem. Soc.* **2004**, *126*, 2658.
[29] S. Bhattacharjee, D. M. Dotzauer, M. L. Bruening, *J. Am. Chem. Soc.* **2009**, *131*, 3601.
[30] J. Gao, Q. Liu, F. Gu, B. Liu, Z. Zhong, F. Su, *RSC Adv.* **2015**, *5*, 22759.
[31] S. Tada, R. Kukuchi, *Catal. Sci. Technol.* **2015**, *5*, 3061.
[32] Z. Sun, L. Zhang, F. Dang, Y. Liu, Z. Fei, Q. Shao, H. Lin, J. Guo, L. Xiang, N. Yerra, Z. Guo, *CrystEngComm* **2017**, *19*, 3288.
[33] Y. Zheng, Y. Zheng, S. Yang, Z. Guo, T. Zhang, H. Song, Q. Shao, *Green Chem. Lett. Rev.* **2017**, *10*, 202.
[34] C. Wang, Y. Wu, Y. Li, Q. Shao, X. Yan, C. Han, Z. Wang, Z. Liu, Z. Guo, *Polym. Adv. Technol.* https://doi.org/10.1002/pat.4105.
[35] D. Reith, B. Müller, F. Müller-Plathe, S. Wiegand, *J. Chem. Phys.* **2002**, *116*, 9100.
[36] B. Wang, Y.-P. Wang, P. Zhou, Z.-Q. Liu, S.-Z. Luo, W. Chu, Z. Guo, *Colloids Surf. A* **2017**, *514*, 168.
[37] Y. Wang, W. Li, X. Jiao, D. J. Chen, *Mater Chem. A* **2013**, *1*, 10720.
[38] B.-S. Yeo, Z.-H. Chen, W.-S. Sim, *Langmuir* **2003**, *19*, 2787.
[39] Y. Wang, W. Li, Y. Xia, X. Jiao, D. J. Chen, *Mater Chem. A* **2014**, *2*, 15124.
[40] Y. Mao, B. M. Fung, *J. Colloid Interface Sci.* **1997**, *191*, 216.
[41] M. Wiśniewska, S. Chibowski, T. Urban, *J. Colloid Interface Sci.* **2009**, *334*, 146.
[42] A. Malgat, J.-P. Boisvert, C. Daneault, *J. Colloid Interface Sci.* **2004**, *269*, 320.
[43] Y. G. Mishael, P. L. Dubin, R. de Vries, A. B. Kayitmazer, *Langmuir* **2007**, *23*, 2510.
[44] D. Hu, J. Gao, Y. Ping, L. Jia, P. Gunawan, Z. Zhong, G. Xu, F. Gu, F. Su, *Ind. Eng. Chem. Res.* **2012**, *12*, 4875.
[45] Z. Xu, N. Wang, W. Chu, J. Deng, S. Luo, *Catal. Sci. Technol.* **2015**, *5*, 1588.
[46] L. Liu, P. Bernazzani, W. Chu, S.-Z. Luo, B. Wang, Z. Guo, *Adv. Compos. Hybrid Mater.* accepted.
[47] L. Zhang, W. Yu, C. Han, J. Guo, Q. Zhang, H. Xie, Q. Shao, Z. Sun, Z. Guo, *J. Electrochem. Soc.* **2017**, *164*, H651.
[48] Y. Li, X. Wu, J. Song, J. Li, Q. Shao, N. Cao, N. Lu, Z. Guo, *Polymer* **2017**, *124*, 41.

[49] W. Yang, X. Wang, J. Li, X. Yan, S. Ge, S. Tadakamalla, Z. Guo, *Polym. Eng. Sci.* **2017**, https://doi.org/10.1002/pen.24675.
[50] T. Wu, Q. Shao, S. Ge, *RSC Adv.* **2016**, *6*, 58020.
[51] W. Zhu, S. Ge, Q. Shao, *RSC Adv.* **2016**, *6*, 81736.
[52] K. Sun, P. Xie, Z. Wang, T. Su, Q. Shao, J. Ryu, X. Zhang, J. Guo, A. Shankar, J. Li, R. Fan, D. Cao, Z. Guo, *Polymer* **2017**, *125*, 50.
[53] J. Zhang, Q. Kong, L. Yang, D. Wang, *Green Chem.* **2016**, *18*, 3066.
[54] S. Ge, X. Yang, Q. Shao, Q. Liu, T. Wang, L. Wang, X. Wang, *J. Solid State Chem.* **2013**, *200*, 136.
[55] J. Guo, H. Song, H. Liu, C. Luo, Y. Ren, T. Ding, M. Khan, D. Young, X. Liu, X. Zhang, J. Kong, Z. J. Guo, *Mater. Chem. C* **2017**, *5*, 5334.
[56] X. Guan, G. Zheng, K. Dai, C. Liu, X. Yan, C. Shen, Z. Guo, *ACS Appl. Mater. Inter.* **2016**, *8*, 14150.
[57] Y. Ma, L. Lyu, Y. Guo, Y. Fu, Q. Shao, T. Wu, S. Guo, K. Sun, X. Guo, E. K. Wujcik, Z. Guo, *Polymer* accepted.
[58] J. Huang, Y. Cao, Q. Shao, X. Peng, Z. Guo, *Ind. Eng. Chem. Res.* https://doi.org/10.1021/acs.iecr.7b02835.
[59] Z. Wu, S. Gao, L. Chen, D. Jiang, Q. Shao, B. Zhang, Z. Zhai, C. Wang, M. Zhao, Y. Ma, X. Zhang, L. Weng, M. Zhang, Z. Guo, *Macromol. Chem. Phys.* accepted.
[60] X. Lou, C. Lin, Q. Luo, J. Zhao, B. Wang, J. Li, Q. Shao, X. Guo, N. Wang, Z. Guo, *ChemElectroChem*. https://doi.org/10.1002/celc.201700816.
[61] K. Zhang, G. Li, L. Feng, N. Wang, J. Guo, K. Sun, K. Yu, J. Zeng, T. Li, Z. Guo, M. J. Wang, *Mater. Chem. C*. https://doi.org/10.1039/c7tc02948a.
[62] T. Liu, K. Yu, L. Gao, H. Chen, N. Wang, L. Hao, T. Li, H. He, Z. J. Guo, *Mater. Chem. A* **2017**, *5*, 17848.

How to cite this article: Zhou P, Wang S, Tao C, et al. PAA/alumina composites prepared with different molecular weight polymers and utilized as support for nickel-based catalyst. *Adv Polym Technol*. 2018;37: 2325–2335. https://doi.org/10.1002/adv.21908